Liquid Crystals
Publication details, including instructions for authors and subscription information:
http://www.informaworld.com/smpp/title~content=t713926090

Infrared spectroscopic and mesomorphic studies of 4,4'-bis(?-hydroxyalkoxy)-a-methylstilbenes

Chieh-Hao Wan; Jen-Feng Kuo

Online publication date: 06 August 2010

To cite this Article Wan, Chieh-Hao and Kuo, Jen-Feng(2001) 'Infrared spectroscopic and mesomorphic studies of 4,4'-bis(?-hydroxyalkoxy)-a-methylstilbenes', Liquid Crystals, 28: 4, 535 — 548
To link to this Article: DOI: 10.1080/02678290010010112
URL: http://dx.doi.org/10.1080/02678290010010112

LIQUID CRYSTALS, 2001, VOL. 28, NO. 4, 535–548

Infrared spectroscopic and mesomorphic studies of 4,4′-bis(ω-hydroxyalkoxy)-α-methylstilbenes

CHIEH-HAO WAN and JEN-FENG KUO*

Department of Chemical Engineering, National Cheng-Kung University, Tainan, Taiwan 701, Taiwan ROC

(*Received 21 June 2000; in final form 8 August 2000; accepted 4 September 2000*)

Two liquid crystal materials, 4,4′-bis(ω-hydroxyalkoxy)-α-methylstilbenes, with butyloxy and octyloxy terminal chains and denoted HAMS-4 and HAMS-8, respectively, were synthesized. The corresponding compounds, 4,4′-bis(ω-alkoxy)-α-methylstilbenes (AMS-*n*) (*n* = 2 to 7, 9, 10 and 11), which do not hydrogen bond, were also synthesized and used to study the influence of hydrogen bonding on phase behaviour. DSC, polarizing optical microscopy and miscibility studies were used for determination of the structure and property relationships of the various liquid crystalline phases exhibited by the two homologues and the AMS-*n* homologues. The FTIR spectra were measured at various temperatures on going from the crystalline phase to the isotropic phase through the intermediate phases. The characteristics of the OH stretch band, the CH_2 stretching, bending and rocking progression modes, as well as the ring C=C stretch and the ring skeletal vibrations were studied to elucidate the modes and geometry of the hydrogen bonding of the terminal OH group, the conformation of the terminal chains and the intermolecular interaction between the aromatic mesogenic cores in the various phases.

1. Introduction

The usefulness of vibrational infrared and Raman spectroscopy as structural probes for the study of the molecular microstructure has already been demonstrated in the cases of molecules which contain conformationally flexible residues [1–3]. This spectroscopic technique has been successfully used by Zerbi and coworkers in the study of the various phases shown by the mesogens dodecylcyanobiphenyl and dodecyloxycyanobiphenyl [4, 5]. The results showed that the vibrational spectra provide specific and direct information related to the local, as well as to the overall molecular structure. Hsu and coworkers [6] used vibrational spectroscopy to analyse the microstructures of three disk-like crystalline macromolecules and suggested that the structures of the polymethylene sequences are correlated with the phase behaviour.

Hydrogen bonding has been shown to play an important role in the formation of liquid crystals and thereby influence the liquid crystalline properties [7–14]. Macknight and coworkers [15] utilized infrared spectroscopy to study the changes that occur both in the conformation of the alkyl chains, as well as the mobility of the mesogen and the alkyl chains in the various phases of 4,4′-bis(6-hydroxyhexyloxy)biphenyl (BHHBP), which gave rise to hydrogen bonding involving the terminal chains with the hydroxyl group. Recently, Li and coworkers [14] studied the effect of hydrogen bonding on the phase behaviours of *p*-nitroazobenzene derivatives with hydrophilic tails (OH group) by using Fourier transform infrared (FTIR) spectroscopy. They showed that the existence of intermolecular hydrogen bonding between the OH groups and the strong dipolar interactions of the NO_2 group resulted in the high stability and the high orientational ordering properties of the *N*-(4-nitrophenyl)azophenyloxyalkyldiethanolamines (C*n*) in the liquid crystalline state compared with the bromo-1-[4-(4-nitrophenyl)azophenyl]oxyalkanes (B*n*).

In a previous publication [16], we reported the synthesis and mesomorphism of the 4,4′-bis(ω-hydroxyalkoxy)-α-methylstilbenes, denoted HAMS-*n*, where *n* is the carbon atom length of the terminal *n*-alkyl chains. In the present work, two typical members of the HAMS-*n* homologues, HAMS-4 and HAMS-8, which were anticipated to be hydrogen-bonded compounds, were studied. A corresponding series of compounds with a methyl group at the terminus of the end chain, 4,4′-bis(ω-alkoxy)-α-methylstilbene (AMS-*n*) homologues (*n* = 2 to 7, 9, 10 and 11), which do not hydrogen bond, were also synthesized in order to compare the importance of the effect of hydrogen bonding on the liquid crystalline behaviours. The structure and thermotropic properties of the compounds were determined. The FTIR spectra were measured

*Author for correspondence; e-mail: jenfkuo@mail.ncku.edu.tw

Liquid Crystals ISSN 0267-8292 print/ISSN 1366-5855 online © 2001 Taylor & Francis Ltd
http://www.tandf.co.uk/journals
DOI: 10.1080/02678290010010112

as a function of temperature. The hydrogen bonding related bands, as well as the conformation related bands in the fingerprint region were correlated with the phase states, the conformations of the terminal chains and the intermolecular interactions between the aromatic mesogenic cores in the various phases. The molecular structures of HAMS-*n* and AMS-*n* are shown in figure 1.

2. Experimental

2.1. *Characterization techniques*

The ^{1}H NMR spectra of all products were recorded (Bruker AMX 400 MHz) using tetramethylsilane (TMS) as an internal chemical shift reference. Elemental analyses were carried out using a Heraeus CHN-O-RAPID elemental analyser. IR spectra were measured using a Bio-Rad, FTS-40A, FTIR spectrometer; the samples for general study were pressed KBr discs. The thermal properties were characterized by differential scanning calorimetry (Du Pont 910 with RCS) at a scan rate of 5°C min^{-1} in the temperature range from 0°C to above the clearing points. The peak maxima were taken as phase transition temperatures. Optical textures of the liquid crystalline phases were observed using an Olympus BH-2 polarizing optical microscope (POM) equipped with a LINKAM THMS 600 hot stage and a TMS 91 temperature control system.

The software of the FTIR spectrometer allows numerical handling of the data and was used for numerical integration, spectral subtraction, band fitting, etc. This study has been carried out by recording the spectra with increasing temperature from ambient through the various phase transitions. For infrared measurements, the sample was placed between two KBr windows. This cell was then heated in an electric oven with the temperature measured by a thermocouple estimated to be accurate within ± 1°C. All spectra were taken with a

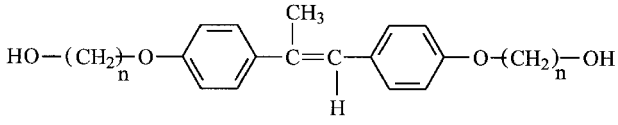

HAMS-n (n= 2,3,4,5,6,7,8,11)

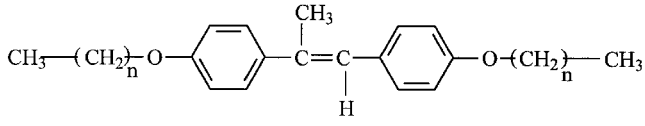

AMS-n (n= 2,3,4,5,6,7,9,10,11)

Figure 1. The molecular structures of HAMS-*n* and AMS-*n*.

2 cm^{-1} spectral resolution. Generally, 64 scans were signal-averaged to obtain a very high signal-to-noise ratio.

The polycrystalline samples were obtained directly in the cell by crystallization from the melt. It must be pointed out that we have also extensively recorded and studied the infrared spectra of solid samples as KBr pellets. In these cases, the spectra are more structured and do not show the expected features of a solid or a liquid organic compound. Thus, in this work, we have studied only solids crystallized from the melt in the cell.

2.2. *Synthesis*

2.2.1 *4,4′-Bis(8-hydroxyoctyloxy)-α-methylstilbene (HAMS-8) and 4,4′-bis(4-hydroxybutyloxy)-α-methylstilbene (HAMS-4)*

The detailed synthetic routes for HAMS-8 and HAMS-4 have been given previously [16, 17–19]. ^{1}H NMR and elemental analysis results were as follows:

HAMS-8. ^{1}H NMR (400 MHz, DMSO-d$_6$): δ 1.23–1.42 (m, 20H), 1.67–1.74 (m, 4H), 2.17 (s, 3H), 3.36–3.41 (m, 4H, −C<u>H</u>$_2$−OH), 3.95–3.98 (t, 4H, −Ph−O−C<u>H</u>$_2$−), 4.12–4.15 (t, 2H, −CH$_2$−O<u>H</u>), 6.71 (s, 1H), 6.88–6.92 (m, 4H, aromatic protons, *o* to −OH), 7.26–7.28 (d, 2H, aromatic protons, *o* to α-CH$_3$), 7.42–7.44 (d, 2H, aromatic protons, *o* to =CH). FTIR (KBr): 3326, 2933, 2855, 1607, 1571, 1514, 1475, 1382, 1279,1254, 1074, 1033, 722 cm^{-1}. Elemental analysis: found C 77.16, H 9.49; calc. for $C_{31}H_{46}O_4$ C 77.14, H 9.61%.

The results for HAMS-4 were:

HAMS-4. ^{1}H NMR (400 MHz, acetone-d$_6$): δ 1.66–1.69 (m, 4H), 1.83–1.85 (m, 4H), 2.23 (s, 3H), 3.55–3.57 (m, 2H, −CH$_2$−O<u>H</u>), 3.61–3.64 (m, 4H, −C<u>H</u>$_2$−OH), 4.04 (m, 4H, −Ph−O−C<u>H</u>$_2$−), 6.76 (s, 1H), 6.93–6.95 (m, 4H, aromatic protons, *o* to −OH), 7.30–7.33 (d, 2H, aromatic protons, *o* to α-CH$_3$), 7.46–7.50 (d, 2H, aromatic protons, *o* to =CH). FTIR (KBr): 3307, 2944, 2910, 2875, 1606, 1513, 1477, 1397, 1380, 1279 1251, 1233, 1075, 1049, 1019, 745 cm^{-1}. Elemental analysis: found C 74.52, H 8.06; calc. for $C_{23}H_{30}O_4$ C 74.56, H 8.16%.

2.2.2. *4,4′-Bis(ω-alkoxy)-α-methylstilbenes (AMS-n) (n = 2, 3, 4, 5, 6, 7, 9, 10, 11)*

The AMS-*n* homologues were synthesized by similar procedures; here *n* is the number of methylene units. A typical synthetic procedure for AMS-5 is illustrated as follows. HMS (1 mol), KOH (4 mol), KI (0.03 mol) and 250 ml ethanol were placed in a four-necked reactor and heated to 78°C. 1-Chlorohexane (3.5 mol) was added drop-wise to the well stirred solution. The reaction mixture was then heated under reflux for 48 h. After cooling to 0°C, the mixture was filtered and the solid material washed with water and NaOH solution to remove unreacted matter. A white crystalline product was

obtained by recrystallization of the solid product from ethanol or dioxan. Yields: 58%. ^{1}H NMR (400 MHz, acetone-d_6): δ 0.87–0.94 (t, 6H, $-C\underline{H}_3$), 1.33–1.48 (m, 12H, $-C\underline{H}_2-$), 1.71–1.81 (m, 4H, $-O-CH_2-C\underline{H}_2-$), 2.23 (S, 3H, α-$C\underline{H}_3$), 3.97–4.04 (t, 4H, $-O-C\underline{H}_2$), 6.76 (s, 1H, $=C\underline{H}$), 6.90–6.96 (m, 4H, aromatic protons, *m* to α-CH_3), 7.29–7.33 (d, 2H, aromatic protons, *o* to α-CH_3), 7.49–7.50 (d, 2H, aromatic protons, *o* to =CH). Elemental analysis: found C 82.19, H 9.73; calc. for $C_{27}H_{38}O_2$ C 82.18, H 9.71%.

Table 1. Yields and elemental analysis results for the 4,4′-bis(ω-alkoxy)-α-methylstilbenes (AMS-*n*).

	Calculated/%		Found/%		
Homologue	C	H	C	H	Yield/%
AMS-2	81.25	8.44	81.14	8.47	51
AMS-3	81.61	8.93	81.54	9.01	55
AMS-4	81.92	9.35	81.88	9.35	56
AMS-5	82.18	9.71	82.19	9.73	58
AMS-6	82.41	10.01	82.39	10.02	52
AMS-7	82.61	10.28	82.52	10.25	55
AMS-9	82.95	10.74	82.95	10.67	60
AMS-10	83.08	10.93	83.03	10.87	61
AMS-11	83.21	11.10	83.16	11.19	60

Using similar methods, the other AMS-*n* homologues were synthesized. The elemental analyses and ^{1}H NMR data for the other homologues are given in tables 1 and 2.

2.2.3. *4-Octyloxy-4′-cyanobiphenyl (8OCB)*

The method suggested by Goodby [20] was adopted for the preparation of the standard mesogen 4-octyloxy-4′-cyanobiphenyl (8OCB). Elemental analysis: found C 81.89, H 8.21, N 4.52; calc. for $C_{21}H_{25}NO$ C 82.04, H 8.20, N 4.56%.

The product had the following transition temperatures in agreement with the literature: Cr–54°C–SmA–67°C–N–80°C–I (lit. Cr–54°C–SmA–67°C–N–80°C–I [21]).

2.2.4. *4,4′-Bis(6-hydroxyhexyloxy)biphenyl (BHHBP)*

This compound was prepared according to the method of Ringsdorf and coworkers [15, 22, 23]. Elemental analysis: found C 74.48, H 8.76; calc. for $C_{24}H_{34}O_4$ C 74.58, H 8.86%.

Table 2. ^{1}H NMR chemical shifts obtained at room temperature for the AMS-*n* homologues.

Homologue	^{1}H NMR (400 MHz, ppm)
AMS-2	(Acetone-d_6) 0.87–0.94 (t, 6H, $-C\underline{H}_3$), 1.71–1.81 (m, 4H, $-O-CH_2-C\underline{H}_2-$), 2.23 (S, 3H, α-$C\underline{H}_3$), 3.97–4.04 (t, 4H, $-O-C\underline{H}_2$), 6.76 (s, 1H, $=C\underline{H}$), 6.90–6.96 (m, 4H, aromatic protons, *m* to α-CH_3), 7.29–7.33 (d, 2H, aromatic protons, *o* to α-CH_3), 7.49–7.50 (d, 2H, aromatic protons, *o* to =CH).
AMS-3	(Acetone-d_6) 0.87–0.94 (t, 6H, $-C\underline{H}_3$), 1.33–1.48 (m, 4H, $-C\underline{H}_2-$), 1.71–1.81 (m, 4H, $-O-CH_2-C\underline{H}_2-$), 2.23 (S, 3H, α-$C\underline{H}_3$), 3.97–4.04 (t, 4H, $-O-C\underline{H}_2$), 6.76 (s, 1H, $=C\underline{H}$), 6.90–6.96 (m, 4H, aromatic protons, *m* to α-CH_3), 7.29–7.33 (d, 2H, aromatic protons, *o* to α-CH_3), 7.49–7.50 (d, 2H, aromatic protons, *o* to =CH).
AMS-4	(Acetone-d_6) 0.87–0.94 (t, 6H, $-C\underline{H}_3$), 1.33–1.48 (m, 8H, $-C\underline{H}_2-$), 1.71–1.81 (m, 4H, $-O-CH_2-C\underline{H}_2-$), 2.23 (S, 3H, α-$C\underline{H}_3$), 3.97–4.04 (t, 4H, $-O-C\underline{H}_2$), 6.76 (s, 1H, $=C\underline{H}$), 6.90–6.96 (m, 4H, aromatic protons, *m* to α-CH_3), 7.29–7.33 (d, 2H, aromatic protons, *o* to α-CH_3), 7.49–7.50 (d, 2H, aromatic protons, *o* to =CH).
AMS-5	(Acetone-d_6) 0.87–0.94 (t, 6H, $-C\underline{H}_3$), 1.33–1.48 (m, 12H, $-C\underline{H}_2-$), 1.71–1.81 (m, 4H, $-O-CH_2-C\underline{H}_2-$), 2.23 (S, 3H, α-$C\underline{H}_3$), 3.97–4.04 (t, 4H, $-O-C\underline{H}_2$), 6.76 (s, 1H, $=C\underline{H}$), 6.90–6.96 (m, 4H, aromatic protons, *m* to α-CH_3), 7.29–7.33 (d, 2H, aromatic protons, *o* to α-CH_3), 7.49–7.50 (d, 2H, aromatic protons, *o* to =CH).
AMS-6	(Acetone-d_6) 0.87–0.94 (t, 6H, $-C\underline{H}_3$), 1.33–1.47 (m, 16H, $-C\underline{H}_2-$), 1.71–1.81 (m, 4H, $-O-CH_2-C\underline{H}_2-$), 2.23 (S, 3H, α-$C\underline{H}_3$), 3.97–4.04 (t, 4H, $-O-C\underline{H}_2$), 6.76 (s, 1H, $=C\underline{H}$), 6.90–6.96 (m, 4H, aromatic protons, *m* to α-CH_3), 7.29–7.33 (d, 2H, aromatic protons, *o* to α-CH_3), 7.49–7.50 (d, 2H, aromatic protons, *o* to =CH).
AMS-7	($CDCl_3$) 0.85–0.92 (t, 6H, $-C\underline{H}_3$), 1.30–1.47 (m, 20H, $-C\underline{H}_2-$), 1.72–1.82 (m, 4H, $-O-CH_2-C\underline{H}_2-$), 2.24 (s, 3H, α-$C\underline{H}_3$), 3.94–4.00 (t, 4H, $-O-C\underline{H}_2-$), 6.71 (s, 1H, $=C\underline{H}$), 6.85–6.91 (m, 4H, aromatic protons, *m* to α-CH_3), 7.25–7.29 (d, 2H, aromatic protons, *o* to α-CH_3), 7.41–7.45 (d, 2H, aromatic protons, *o* to =CH).
AMS-9	($CDCl_3$) 0.85–0.92 (t, 6H, $-C\underline{H}_3$), 1.30–1.47 (m, 28H, $-C\underline{H}_2-$), 1.72–1.82 (m, 4H, $-O-CH_2-C\underline{H}_2-$), 2.24 (s, 3H, α-$C\underline{H}_3$), 3.94–4.00 (t, 4H, $-O-C\underline{H}_2-$), 6.71 (s, 1H, $=C\underline{H}$), 6.85–6.91 (m, 4H, aromatic protons, *m* to α-CH_3), 7.25–7.29 (d, 2H, aromatic protons, *o* to α-CH_3), 7.41–7.45 (d, 2H, aromatic protons, *o* to =CH).
AMS-10	($CDCl_3$) 0.85–0.92 (t, 6H, $-C\underline{H}_3$), 1.27–1.45 (m, 32H, $-C\underline{H}_2-$), 1.75–1.79 (m, 4H, $-O-CH_2-C\underline{H}_2-$), 2.24 (s, 3H, α-$C\underline{H}_3$), 3.94–4.00 (t, 4H, $-O-C\underline{H}_2-$), 6.71 (s, 1H, $=C\underline{H}$), 6.85–6.91 (m, 4H, aromatic protons, *m* to α-CH_3), 7.25–7.29 (d, 2H, aromatic protons, *o* to α-CH_3), 7.41–7.45 (d, 2H, aromatic protons, *o* to =CH).
AMS-11	($CDCl_3$) 0.85–0.92 (t, 6H, $-C\underline{H}_3$), 1.28–1.46 (m, 36H, $-C\underline{H}_2-$), 1.72–1.82 (m, 4H, $-O-CH_2-C\underline{H}_2-$), 2.24 (s, 3H, α-$C\underline{H}_3$), 3.94–4.00 (t, 4H, $-O-C\underline{H}_2-$), 6.71 (s, 1H, $=C\underline{H}$), 6.85–6.91 (m, 4H, aromatic protons, *m* to α-CH_3), 7.25–7.29 (d, 2H, aromatic protons, *o* to α-CH_3), 7.41–7.45 (d, 2H, aromatic protons, *o* to =CH).

The product had the phase transition temperatures: Cr–97°C–CrG(or CrH)–173°C–I (lit. Cr–98°C–CrG (or CrH)–179°C–I [15]).

3. Results and discussion

3.1. *Mesomorphism of HAMS-n homologues*

Phase transition temperatures and entropy changes for the HAMS-*n* homologues were reported previously [16], and are listed for reference in table 3. Two typical members of the HAMS-*n* homologues, HAMS-4 and HAMS-8, are considered in detail now for their mesomorphism. Typical DSC heating and cooling traces recorded at a rate of 5°C min^{-1} for HAMS-4 and HAMS-8 are shown in figure 2. HAMS-4 shows three endothermic peaks (75, 139 and 153°C) on heating and three exothermic peaks (69, 129 and 148°C) on cooling. HAMS-8 gives two endothermic peaks (77 and 134°C) on heating and two exothermic peaks (68 and 125°C) on cooling. According to the DSC results, HAMS-4 and -8 may be regarded as enantiotropic dimorphic and monomorphic mesogens, respectively. However, POM of HAMS-4 subsequently revealed on cooling a texture of droplets with a cross at 157°C, a focal-conic fan texture at 148°C, a mosaic texture at 129°C and a mosaic texture with a fracture pattern below 69°C. The same textures also form on heating. Accordingly, HAMS-4 exhibits enantiotropic trimorphism including the upper nematic phase, a smectic phase with a focal-conic fan texture and another phase with a mosaic texture, and not dimorphism as indicated by DSC. This must be due to the extremely small enthalpy change for the I–N phase transition that is not detected by DSC. For

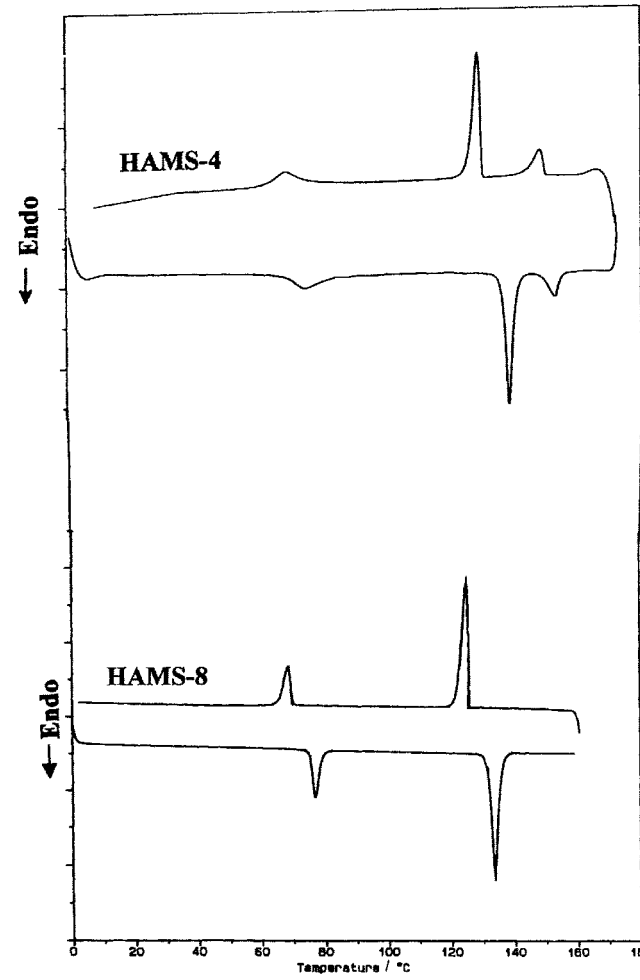

Figure 2. DSC thermograms of HAMS-4 and HAMS-8.

Table 3. Phase transition temperatures (T/°C) and entropy changes (ΔS/J K^{-1} mol^{-1}) for the HAMS-*n* homologues (see figure 1), obtained mainly by DSC. Parentheses indicate values for monotropic phase transitions observed during cooling.

Homologue	Formula		Cr		CrG or CrH		SmA		N		I
HAMS-2	$C_{19}H_{22}O_4$	H[a]	•	103.0/27.5	•	149.3/52.9	•	160.4[c]/10.8	•	165.0[b]	•
		C	•	75[a]/–	•	136.4/64.0	•	156.7/11.1	•	163.5[b]	•
HAMS-3	$C_{21}H_{26}O_4$	H	•							155.5/74.9	•
		C	•	(80.0/–)[b]	•	(144.0/60.2)	•	(153.3/15.1)	•	159.1[b]	•
HAMS-4	$C_{23}H_{30}O_4$	H	•	75.3/16.7	•	139.2/50.2	•	153.4/12.2	•	159.2[b]	•
		C	•	69.5/16.5	•	129.5/52.7	•	148.8/12.8	•	157.3[b]	•
HAMS-5	$C_{25}H_{34}O_4$	H	•							132.9/69.0	•
		C	•	(70.0/–)[b]	•	(117.7/55.7)	•	(127.6/7.6)	•	137.0[b]	•
HAMS-6	$C_{27}H_{38}O_4$	H	•	77.6/49.7	•	133.3/82.0	•	137.8/20.8	•	140.5[b]	•
		C	•	71.7/45.9	•	121.9/97.2	•	135.0/22.6	•	138.6[b]	•
HAMS-7	$C_{29}H_{42}O_4$	H	•							134.8/113.9	•
		C	•	(55.0/–)[b]	•	(124.0/102.2)	•	(126.9/8.6)	•	128.9[b]	•
HAMS-8	$C_{31}H_{46}O_4$	H	•	76.8/24.2	•					133.8/104.1	•
		C	•	68.4/25.8	•					125.0/104.1	•
HAMS-11	$C_{37}H_{58}O_4$	H	•	72.0/7.1	•					137.0/209.7	•
		C	•	68.5/8.1	•					128.8/215.5	•

[a] H: heating process; C: cooling process.
[b] Phase transition temperatures determined by POM.
[c] From [32], the isotropization temperature of the compound is given as 160°C.

HAMS-8, POM only exhibits on cooling a transition from isotropic to a mosaic texture at 125°C, followed by a mosaic texture with fine striations below 68°C, and the same textures were obtained on heating. The material is therefore an enantiotropic smectogen with a mosaic texture.

Miscibility studies were made to identify the types of the smectic phases mentioned above. 4,4′-Bis(6-hydroxyhexyloxy)biphenyl (BHHBP), reported to give a CrG (or CrH) phase with a mosaic texture and a crystalline phase (Cr) with a fracture pattern [15], and 4-octyloxy-4′-cyanobiphenyl (8OCB) with the well established phase sequence Cr–54°C–SmA–67°C–N–80°C–I [21] were used as standards for the miscibility studies. The phase diagrams of the binary mixtures obtained by DSC and POM in the miscibility study are shown in figures 3 and 4.

Figure 3 shows the phase diagram for the full composition range of binary mixtures of HAMS-8 and BHHBP. The CrG (or CrH) phase forms a continuous phase across the full composition range, indicating that HAMS-8 forms the same mesophase as BHHBP. Therefore, coupled with the DSC data, the variants of mesomorphism for HAMS-8 are, Cr–77°C(24 J K^{-1} mol^{-1})–CrG(or CrH)–134°C(104 J K^{-1} mol^{-1})–I (on heating). The values of the entropy changes (ΔS) are given in parenthesis.

Figure 4 presents the phase diagram for HAMS-4 and 8OCB. Like the nematic phase, the smectic phase is continuously miscible across the full composition range. Thus, the smectic phase with a focal-conic fan texture shown from 139 to 153°C is a smectic A phase. BHHBP was again chosen as standard for assignment of the smectic phase with a mosaic texture in the temperature range 75 to 139°C. The test material gives a continuous phase across the full composition range for the CrG (or CrH) phase (figure 5). Consequently, HAMS-4 has the trimorphism, Cr–75°C(17 J K^{-1} mol^{-1})–CrG(or CrH)–139°C(50 J K^{-1} mol^{-1})–SmA–153°C(12.2 J K^{-1} mol^{-1})–N–159°C–I (on heating).

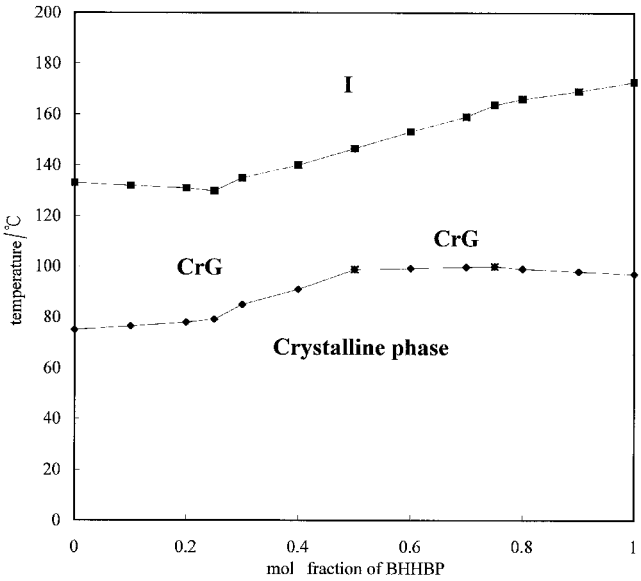

Figure 3. Binary phase diagram of HAMS-8 and 4,4′-bis-(6-hydroxyhexyloxy)biphenyl (BHHBP) (based on heating trace).

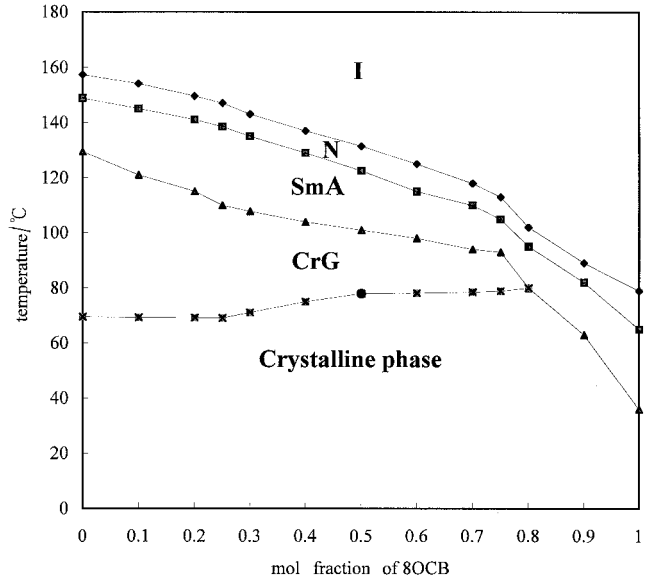

Figure 4. Binary phase diagram of HAMS-4 and 4-octyloxy-4′-cyanobiphenyl (8OCB) (based on cooling traces).

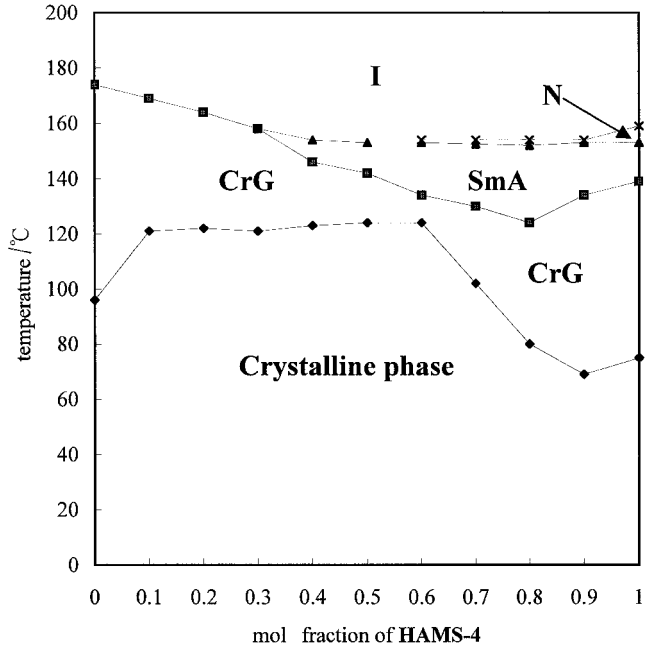

Figure 5. Binary phase diagram of HAMS-4 and 4,4′-bis-(6-hydroxyhexyloxy)biphenyl (BHHBP) (based on heating traces).

From the results, the length of the terminal chain significantly affects the variant of mesomorphism, but has little effect on the temperatures of the crystalline–CrG (or CrH) transition. HAMS-4 has a wider range CrG (or CrH) phase than HAMS-8, 64°C compared with 57°C. MacKnight *et al.* [15] reported that BHHBP was monomorphic CrG (or CrH) with a temperature range of 80°C, but for the HAMS homologues, a terminal chain length of 8 is needed to obtain the single CrG (or CrH) phase; the temperature range of the mesophase is however only 57°C. Obviously, with the biphenyl core it is easier to attain a stable and highly ordered smectic phase than with the α-methylstilbene core.

3.2. *Liquid crystalline properties of the AMS-n homologues*

Figures 6 and 7 present typical DSC thermograms for the AMS-*n* homologues from the second heating and cooling processes recorded at a rate of 5°C min^{-1}. These

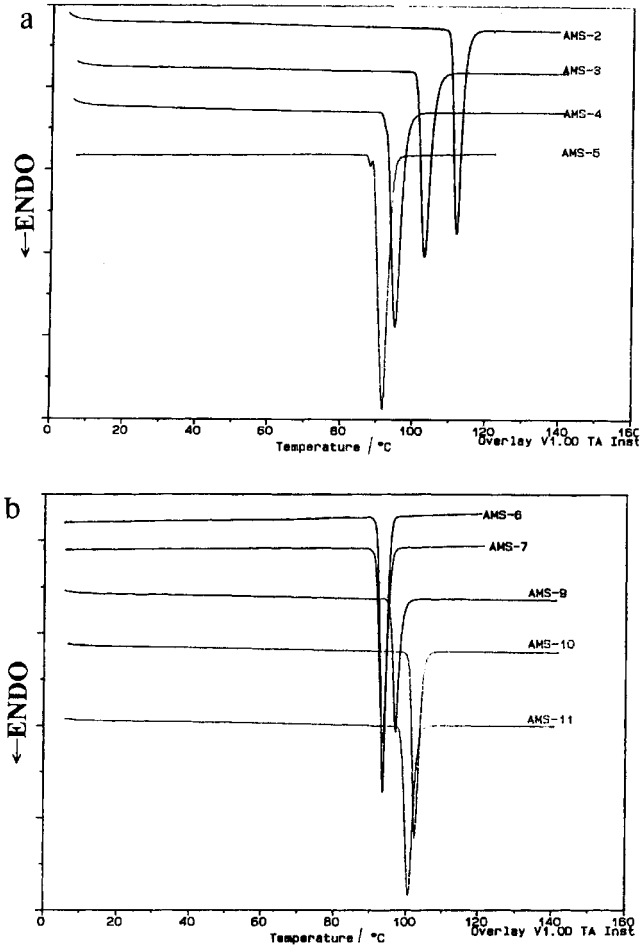

Figure 6. DSC thermograms of the AMS-*n* homologues in the heating process: (*a*) AMS-2, AMS-3, AMS-4, AMS-5, (*b*) AMS-6, AMS-7, AMS-9, AMS-10, AMS-11.

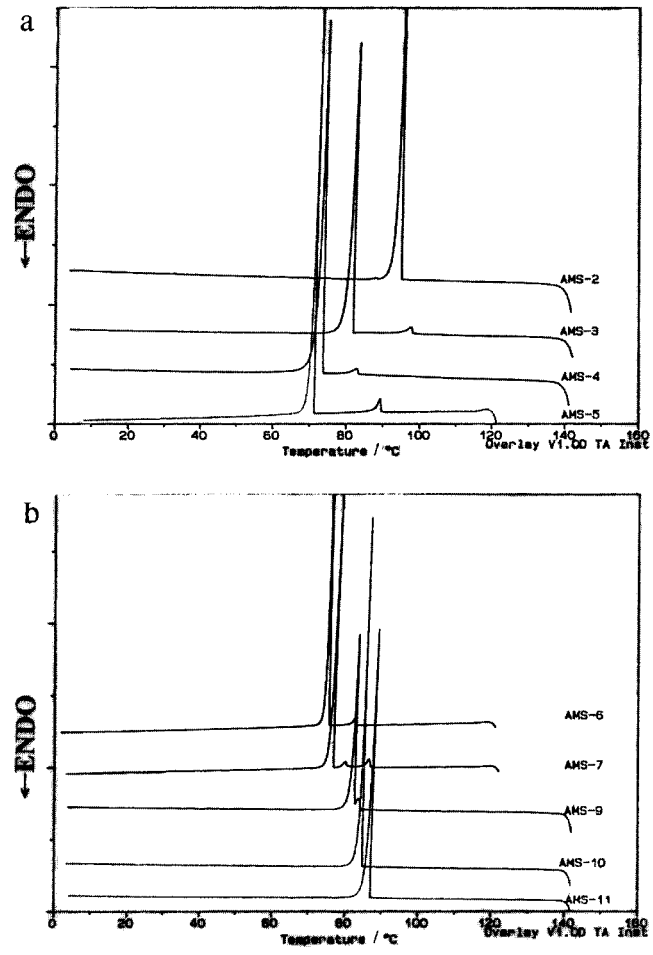

Figure 7. DSC thermograms of the AMS-*n* homologues in the cooling process: (*a*) AMS-2, AMS-3, AMS-4, AMS-5, (*b*) AMS-6, AMS-7, AMS-9, AMS-10, AMS-11.

show one endothermic peak on heating and two exothermic peaks on cooling for AMS-3, 4, 5, 6 and 9, and three exothermic peaks for AMS-7. The other members of the series exhibited one endothermic peak and one exothermic peak on both heating and cooling traces. A typical schlieren texture was observed by POM at the first transition on cooling for the homologues with $n = 3$–9. Thus, the first transition in the DSC cooling trace is the isotropic–nematic phase transition. Consequently, the homologues with $n = 3$–9 exhibited monotropic nematic phases on cooling. No liquid crystalline behaviour was observed for the homologues with $n = 2$, 10 and 11. Cox and co-workers [24] reported that AMS-2 and AMS-3 showed a monotropic nematic phase on cooling. However, we could not find the mesophase for the homologues with $n = 2$.

Table 4 shows the phase transition temperatures and entropy changes for the series AMS-*n*. Figure 8 presents the plot of the phase transition temperatures versus the number of methylene units (*n*) in the terminal alkyl chain

Table 4. Phase transition temperatures (T/°C) and the entropy changes (ΔS/J K^{-1} mole^{-1}) for the AMS-*n* homologues (see figure 1) obtained by DSC. Parentheses indicate values for monotropic phase transitions observed during cooling.

Homologue		Cr	Sm?[a]	N	I
AMS-2[e]	H[b]	•			109.9[c] •
	C	•			97.4/66.5 •
AMS-3	H	•			99.0[d] •
	C	•		(85.3/75.4) •	(97.3[d]/2.7) •
AMS-4	H	•			92.7 •
	C	•		(79.5/100.3) •	(84.0/2.2) •
AMS-5	H	•			90.4 •
	C	•		(75.5/116.3) •	(90.1/3.5) •
AMS-6	H	•			93.5 •
	C	•		(79.1/162.9) •	(83.8/3.5) •
AMS-7[e]	H	•			92.9 •
	C	•	(79.5/140.6) •	(80.2/3.2) •	(86.7/5.1) •
AMS-9	H	•			95.8 •
	C	•		(83.2/107.5) •	(84.4/10.5) •
AMS-10	H	•			100.7 •
	C	•			88.1/192.8 •
AMS-11	H	•			99.1 •
	C	•			89.4/220.9 •

[a] Query smectic phase.
[b] H: heating process; C: cooling process.
[c] In [24] it is reported that the melting point of the compound is 109°C and that it exhibits a monotropic transition on cooling.
[d] In [24], it is reported that the melting point of the compound is 98°C and that it goes nematic at 97°C on cooling.
[e] This compound exhibited a mesophase over a range of only 0.7°C. It was not possible to determine its type by POM or WAXR measurements. Thus, the mesophase is as Sm? phase.

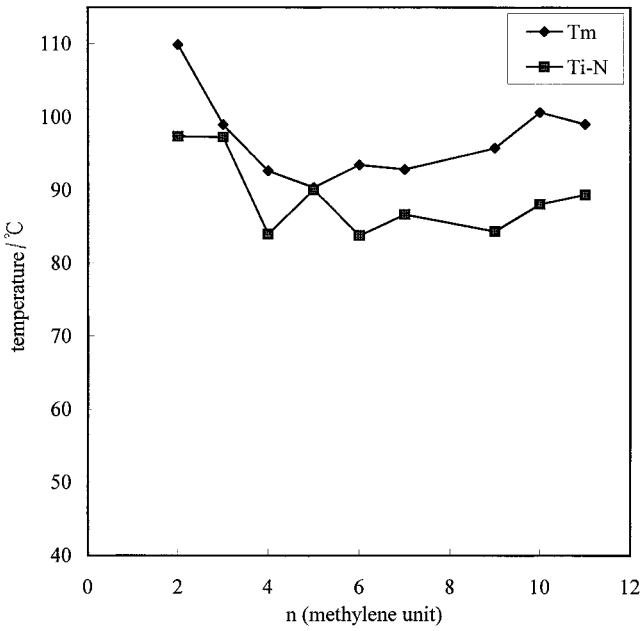

Figure 8. Phase transition temperature vs. the number of methylene units in the terminal alkyl chains of the AMS-*n* homologues.

for the AMS-*n* homologues. The melting temperatures (T_m) decreased as the terminal chain length increased for the homologues with $n = 2$–7, but for $n = 9$–12, T_m slightly increased with increasing n. A significant even–odd effect was found for the isotropic–nematic phase transition temperatures (T_{IN}), the odd numbers of n giving the higher T_{IN}.

The HAMS-*n* phase transition diagram was reported in [16]. In comparison with table 4, one finds that the compounds with end chains terminated with the hydroxyl group (HAMS-*n* homologues) give higher T_m, wider LC phase ranges, enantiotropic behaviour for even values of n and higher orientationally ordered smectic phases (CrG or CrH phase) than those of corresponding AMS-*n* homologues. Obviously, the end groups of the terminal chain significantly influence the liquid crystalline properties, and a study of the hydrogen bonding effect of the terminal hydroxyl group on the phase behaviour of the HAMS-*n* is of interest.

3.3. *The infrared spectra*

Two typical members of the HAMS-*n* series, HAMS-4 and HAMS-8, exhibiting enantiotropic trimorphism for HAMS-4 and monomorphism for HAMS-8, were chosen for a study of the relation between mesomorphism and change in the infrared spectra. Figures 9 and 10 show the FTIR spectra of HAMS-4 and HAMS-8 at various temperatures on going from the crystalline phase to the isotropic phase through the intermediate phases. The tentative assignments for the infrared spectrum of

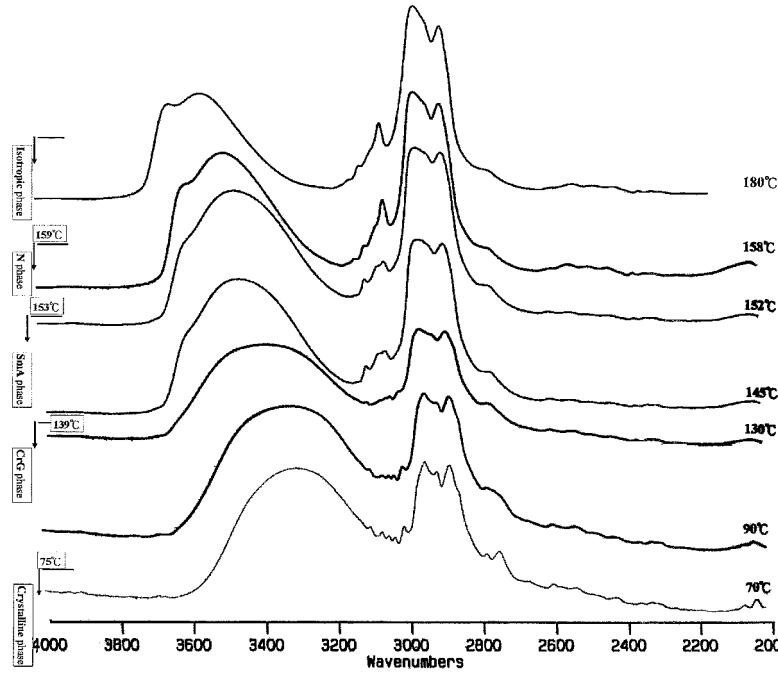

(*a*)

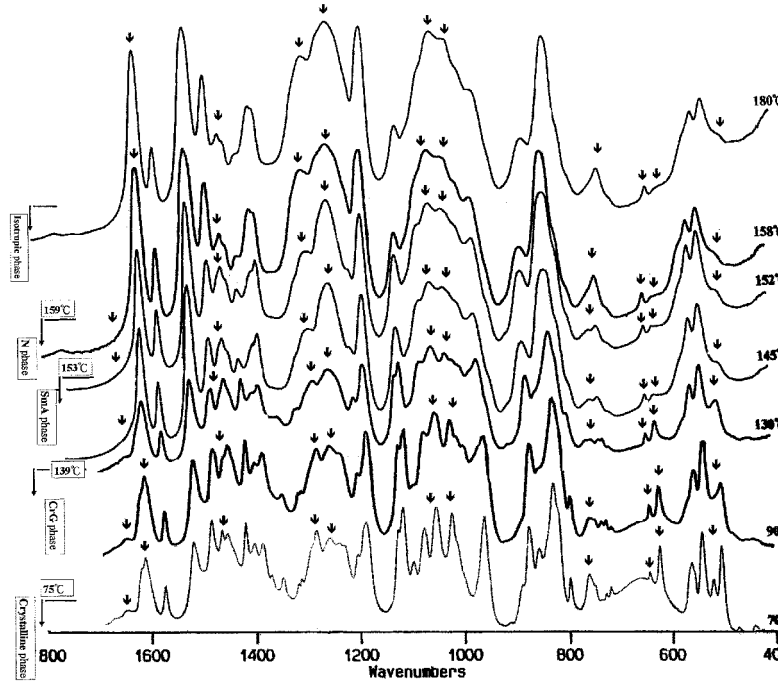

(*b*)

Figure 9. The infrared spectra of HAMS-4 at the indicated temperatures in (*a*) the 2000–4000 cm^{-1} region; (*b*) the 400–1700 cm^{-1} region.

melt-recrystallized HAMS-4 is illustrated in table 5. From the spectra, the conformation of the terminal chains, and the intermolecular interactions of the mesogenic cores, as well as the strength and geometry of the hydrogen bonding of the terminal OH groups with change in the phases will be elucidated.

3.3.1. *The 3600–3300 cm^{-1} region of OH stretch*

First let us focus on the bands appearing in the 3600–3300 cm^{-1} region and arising from the OH stretch vibrations. The hydrogen-bonded OH stretch occurs at around 3300 cm^{-1}, while the free OH stretch occurs at around 3600 cm^{-1} [14, 15, 25–27].

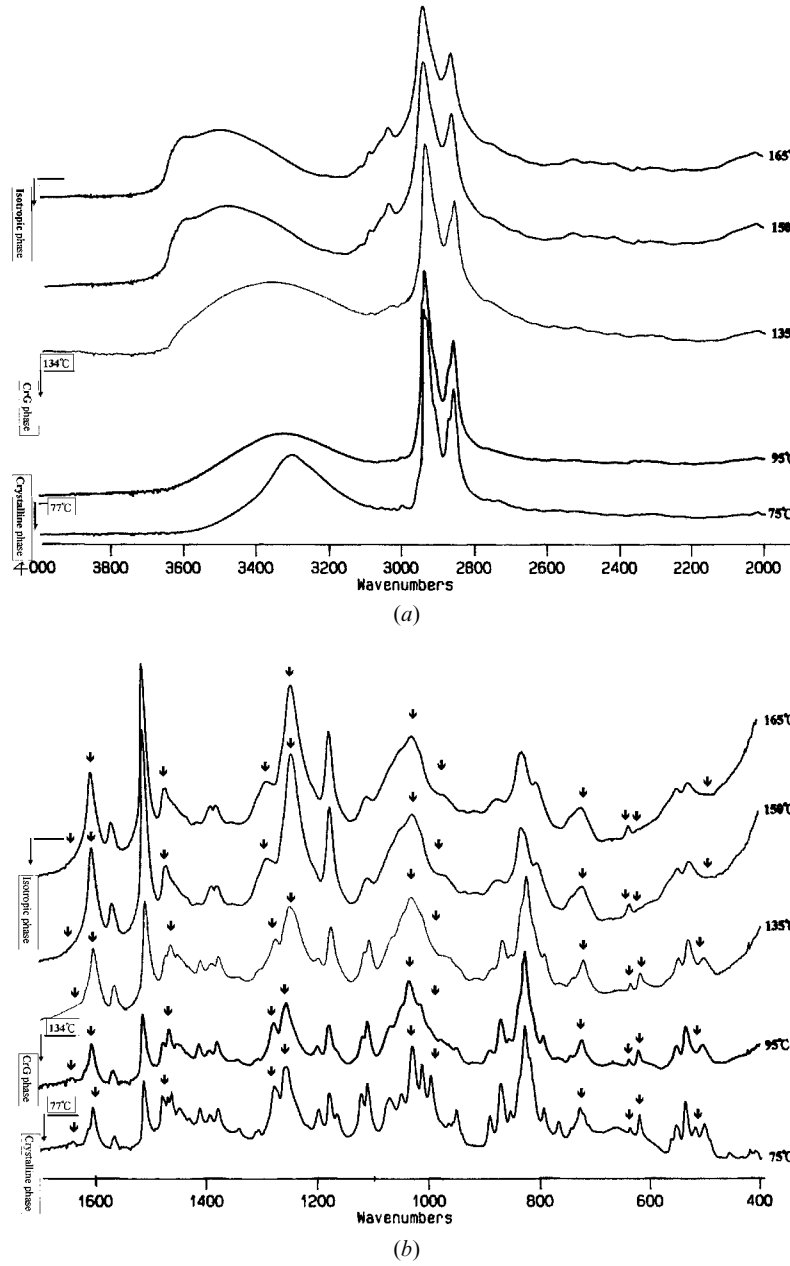

Figure 10. The infrared spectra of HAMS-8 at the indicated temperatures in (*a*) the 2000–4000 cm^{-1} region; (*b*) the 400–1700 cm^{-1} region.

From Figure 9 (*a*), we see that the gross geometry of the OH stretch band of HAMS-4 varies with temperature, especially close to the phase transition temperatures. The band is a Gaussian-like peak below 75°C, and a plateau-like peak between 75 and 139°C. A shoulder on the band appeared about 3550 cm^{-1} between 139°C and 159°C, the peak becoming more of a doublet above the isotropization temperature (> 159°C). Accordingly, the characteristic of the overall band, namely, the band half-width ($\Delta\nu_{1/2}$), was measured as a function of temperature (T). Figure 11 shows the $\Delta\nu_{1/2}$–T plot. $\Delta\nu_{1/2}$ is discontinuous at the crystalline–CrG(or CrH) (*c.* 75°C), the CrG(or CrH)–SmA (*c.* 139°C), and the SmA–N (*c.* 153°C) transitions marked by arrows on the figure. The peak maximum (ν_{max})–T plot was also examined, but the discontinuity in peak maximum is not so remarkable as that for the $\Delta\nu_{1/2}$–T plot.

The deconvolution technique based on the Gaussian model was used for the OH stretch band of HAMS-4 to evaluate for the modes of hydrogen bonding and the integrated intensity (area) in each of the phases. Table 6 summarizes the frequency and the integrated intensity of each mode of hydrogen bonding obtained. The root mean square of the fitting is in the range 3.47×10^{-3} to

Table 5. Tentative qualitative vibrational assignments for the infrared spectrum of melt-recrystallized HAMS-4.

Frequency/cm^{-1}	Group modes
3295	Stretching of OH group with hydrogen bonding
3063, 3002	Stretching of aromatic C−H, ν (C−H).
2944, 2875	Stretching of aliphatic C−H, ν (C−H).
1613, 1606, 1513	Ring C=C stretching
1479, 1459, 1449	CH_3, CH_2 deformation, δ (CH_2), δ (CH_3).
1414	
1397	
1382	C−C−C bending
1278	Hydrogen bonded asymmetric stretching vibration of CH_2−O−H
1254	Stretching vibration of Ph−O−CH_2
1183	
1113	
1071, 1048, 1017	CH_2 rocking progression, P (CH_2).
956	
873	
853	
825	
794, 758, 715	CH_2 rocking progression, P (CH_2).
657	
639	
618	
559, 538, 516, 501	Ring skeletal vibration

9.58×10^{-3}. In general, the band is resolved into two components in the CrG (or CrH) phase (< 139°C). However, upon entering the SmA phase, the shoulder appears, and the overall band is resolved into four components. In the crystalline phase (< 75°C), the two components are 3273–3278 and 3412–3426 cm^{-1}, for which the calculated hydrogen bonding distances are 2.766–2.767 and 2.798–2.801 Å, respectively, increasing with increase in temperature. In the CrG (or CrH) phase, the components are 3288–3338 and 3457–3495 cm^{-1}, for which the hydrogen bonding distances are 2.769–2.781 and 2.808–2.816 Å, respectively, again increasing with temperature. The hydrogen bonding distances obtained by using the Sederholm equation [28], namely, $\Delta\nu(\text{cm}^{-1}) = 4.43 \times 10^3 \ (2.84 - R)$, where $\Delta\nu = \nu$(monomeric OH stretching frequency) − ν (stretching frequency observed in the infrared spectrum of the solid), and ν (monomeric OH stretching frequency) is taken to be 3600 cm^{-1}. The result according to the frequency or the hydrogen bonding distances shows that the terminal OH groups exist in two hydrogen bonding modes in both the crystalline and CrG (or CrH) phases. The two modes of hydrogen bonding do not significantly change their strength with temperature in the crystalline phase. On the contrary, they become significantly weaker with increasing temperature in the CrG (or CrH) phase. Table 7 shows that the ratio of the integrated intensity for the more strongly hydrogen-bonded OH group to that of the weaker hydrogen-bonded OH group, obtained from the area ratio for these two modes of hydrogen bonding, decreases linearly from 3.878 to 3.295 Å with increasing temperature in the crystalline state. It then decreases linearly from 2.205 to 1.827 Å with increasing temperature in the CrG (or CrH) phase. The drastic change in the area ratio in going from the crystalline phase to the CrG (or CrH) phase indicates that each phase is thermodynamically stable within a certain temperature ranges.

Table 6. Deconvoluted results for the OH stretch band of HAMS-4 at various temperatures.

	Components							
Temperature/°C	Peak frequency /cm^{-1}	Area	Peak frequency /cm^{-1}	Area	Peak frequency /cm^{-1}	Area	Peak frequency /cm^{-1}	Area
35	3273	106.112	3412	27.318	—	—	—	—
50	3274	106.432	3416	29.782	—	—	—	—
70	3278	108.260	3426	32.860	—	—	—	—
90	3288	104.720	3457	47.510	—	—	—	—
105	3298	104.850	3468	50.450	—	—	—	—
120	3314	103.984	3482	53.479	—	—	—	—
130	3338	102.446	3495	56.059	—	—	—	—
145	3321	67.274	3425	67.894	3519	57.142	3591	11.399
152	3321	55.250	3434	75.890	3522	45.560	3593	13.947
158	3321	49.030	3439	91.560	3528	39.660	3595	18.820
170	3337	36.445	3460	79.749	3539	29.360	3599	18.247

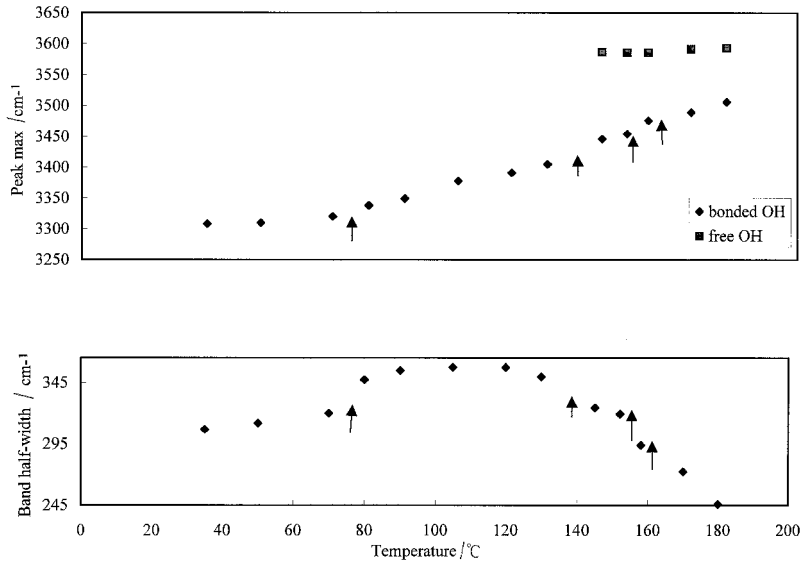

Figure 11. Plot of peak frequency and band half-width for the OH stretch band vs. temperature for HAMS-4.

Table 7. Relative importance of each mode of hydrogen bonding of OH groups for HAMS-4 for the crystalline and CrG (or CrH) phases.

	Modes of hydrogen bonding	
Temperature/°C	$v_{3272\sim3338}/v_{3412\sim3494}$	$v_{3412\sim3494}/v_{3412\sim3494}$
35	3.878	1(0.205)[a]
50	3.574	1(0.219)
70	3.295	1(0.233)
90	2.205	1(0.312)
105	2.077	1(0.325)
120	1.944	1(0.340)
130	1.827	1(0.354)

[a] Parentheses indicate the value of the area ratio of $A_{3412\sim3491}/A_{total}$: ($A_{total} = A_{3412\sim3491} + A_{3272\sim3338}$).

In the range of the SmA and N phases (139 to 159°C), the band resolved into four components, which are at 3321 cm^{-1} (2.777 Å), 3425–3439 cm^{-1} (2.800–2.804 Å), 3519–3528 cm^{-1} (2.822–2.824 Å) and 3591–3595 cm^{-1} (2.840 Å) (table 5), increasing with increase in temperature. The observation of the last two modes indicates that a considerable fraction of the disordering of the molecular arrangement occurred upon entering the SmA phase. Here, the integrated intensity of each mode of hydrogen bonding of the OH groups was calculated with reference to the free OH component (table 8). Upon entering the isotropic phase (> 159°C), the first and third modes still are twice as intense as the free OH component, and the second mode is about 4.9 times the intensity of the free OH mode. Even at 170°C, 12°C higher than the isotropization temperature, the sum for the first and second modes is still larger than those for the third and the last modes, indicating that the hydrogen bonding still persisted in the isotropic phase.

Figure 10(*a*) shows the spectra for the OH stretch of HAMS-8. Below 77°C (in the crystalline phase), the band is centred at 3306 cm^{-1}, and is not a usual Gaussian curve. In the CrG (or CrH) phase, the band shifted to 3347 cm^{-1} (at 95°C) and became a typical Gaussion curve. As the temperature increased to near the CrG (or CrH)–I transition (135°C), the band shifted to 3390 cm^{-1} and a shoulder appeared at *c.* 3600 cm^{-1}, indicating the formation of free OH groups upon entering the isotropic phase. The results again reveal that the strength and distribution of the hydrogen bonding of the OH groups significantly varies with change of phase. Similarly to HAMS-4, the v_{max}, and $\Delta v_{1/2}$ of the overall band were

Table 8. Relative importance of each mode of hydrogen bonding of OH groups for HAMS-4 at the temperatures indicated.

	Modes of hydrogen bonding			
Temperature/°C	$v_{3591\sim3598}/v_{3591\sim3598}$	$v_{3518\sim3538}/v_{3591\sim3598}$	$v_{3425\sim3460}/v_{3591\sim3598}$	$v_{3320\sim3337}/v_{3591\sim3598}$
145	1(0.056)[a]	5.017	5.956	5.902
152	1(0.073)	3.267	5.441	3.961
158	1(0.095)	2.107	4.865	2.605
170	1(0.111)	1.609	4.371	1.997

[a] Parentheses indicate the value of the area ratio of $A_{3591\sim3598}/A_{total}$: ($A_{total} = A_{3591\sim3598} + A_{3518\sim3538} + A_{3425\sim3460} + A_{3320\sim3337}$).

measured as functions of temperature (figure 12). The $\Delta\nu_{1/2}$–T plot indicates the remarkable discontinuities at the crystalline–CrG (or CrH) (77°C) and the CrG (or CrH)–I transitions (134°C). In the ν_{max}–T plot, the discontinuity at the temperature associated with the phase transitions is again less obvious than in the $\Delta\nu_{1/2}$–T plot.

It may be concluded that the strength and distribution of the hydrogen bonding of the terminal OH groups determine the molecular arrangement in space for the various phases obtained. The band half width and/or the integrated intensity ratio of the modes of hydrogen bonding are a probe for the estimation of the phase transitions.

3.3.2. *The fingerprint region, 400–1700 cm^{-1}*

Figures 9(*b*) and 10(*b*) give the infrared spectra of HAMS-4 and -8 in the fingerprint region at a number of temperatures covering all the phases concerned. First let us focus on the changes in the infrared spectra for the CH_2 bending of HAMS-4. Three bands appeared at 1479, 1460 and 1450 cm^{-1} in the crystalline phase (< 75°C), and the order of their intensities was 1479 > 1460 > 1450 cm^{-1}. As the temperature was increased, the peak frequency shifted towards lower frequencies. The 1460 cm^{-1} band disappeared upon entering the CrG (or CrH) phase, and the 1474 cm^{-1} band was weaker than the 1447 cm^{-1} band. However, upon entering the SmA phase (at 145°C), the 1474 cm^{-1} band became stronger than the 1447 cm^{-1} band. For HAMS-8, the spectra for CH_2 bending show four bands at 1480, 1470, 1463 and 1449 cm^{-1} in the crystalline phase and only three bands at 1466, 1477 and 1452 cm^{-1} in the CrG (or CrH) phase. The order of the intensity of these bands in the CrG phase was 1466 ≫ 1477 ≅ 1452 cm^{-1}. Upon entering the isotropic phase, there is a skew band at 1471 cm^{-1}.

The number and intensity of the bands in the region 1100–1000 and 800–700 cm^{-1}, which is attributed to CH_2 rocking progression modes, again significantly changed with phase state. HAMS-8 showed crystal field splitting at 730 and 722 cm^{-1} in the crystalline phase, indicating that a minimum of four consecutive *trans*-sequences existed [29, 30]; these merged into one band at 724 cm^{-1} in the CrG (or CrH) phase, indicating possibly disordering of the terminal chains. Snyder *et al.* [31] demonstrated that if the polymethylene chains are indeed fully *trans* in conformation, two bands near 2920 and 2855 cm^{-1} are to be expected. Here we obtained two bands at 2926 and 2858 cm^{-1} in the crystal phase. Beyond the crystalline phase, two bands at 2933 and 2856 cm^{-1} were obtained, thus indicating that the terminal chain is not fully extended in conformation in the CrG (or CrH) phase. On the other hand, HAMS-4 does not show similar results, because the methylene units are not long enough to give the spectra. We did not find the presence of *gauche* related bands developing upon entering the mesophase as reported for dodecylcyanobiphenyl by Zerbi and Galbiati [4]. Based on the above observations, it is suggested that the alkyl terminal chains develop some degree of disorder in the CrG (or CrH) phase as compared with the fully *trans*-conformation in the crystalline phase, and do not completely disorder until the isotropic phase is reached.

Consider now the region 1630–1500 cm^{-1}, where the ring C=C stretch occurs, and the region 580–500 cm^{-1}, where the ring skeletal vibration occurs. For the latter,

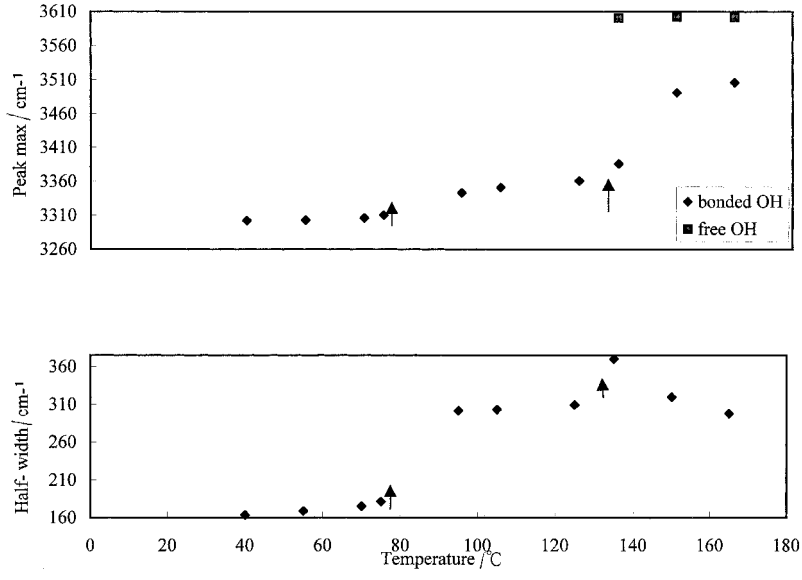

Figure 12. Plot of peak frequency and band half-width for the OH stretch band vs. temperature for HAMS-8.

the crystalline phase exhibited four bands at 559, 538, 516, and 501 cm^{-1} for HAMS-4 and 556, 538, 522, and 504 cm^{-1} for HAMS-8. Among them, the 516 and 522 cm^{-1} bands disappear upon entering the CrG (or CrH) phase, indicating that the corresponding modes of the ring skeletal vibration are closely related to the three-dimensionally ordered structure in the crystalline phase. For HAMS-4, the 501 cm^{-1} band drastically decreased its intensity, and almost lost all intensity upon entering the SmA phase. For HAMS-8, the 504 cm^{-1} band drastically decreased its intensity, and completely disappeared upon entering the isotropic phase. The decrease in intensity of these two bands reveals an increase in the population of conformers with different ring skeletal vibrational mode frequencies. A similar trend was also observed for the changes in the bands for the ring C=C stretch with temperature.

Summarizing the above results, it appears that the molecules develop some positional disorder upon entering the CrG (or CrH) phase, but that the alkyl terminal chains remain predominantly in the *trans*-conformation.

It is found that the band at 1278 cm^{-1}, which is due to the hydrogen-bonded asymmetric stretch of CH_2-O-H [15], is retained into the isotropic temperature. The result is in agreement with that obtained for the OH stretch band. The intensity of the 1278 cm^{-1} band changed relative to that of the $Ph-O-CH_2$ symmetric stretch band at 1254 cm^{-1} for HAMS-4 or at 1258 cm^{-1} for HAMS-8 during increase in the temperature. The deconvolution technique based on the Gaussian model was applied to the two bands to obtain the quantitative integrated intensity ratio, I_{1254}/I_{1278} and I_{1258}/I_{1278}. Figure 13 shows the plots of I_{1254}/I_{1278} and I_{1258}/I_{1278} against temperature. The intensity ratio jumps noticeably near to the temperatures associated with the phase transitions. A similar trend is also found for both the 619 (or 621) and 639 cm^{-1} bands (figure 14).

4. Conclusions

These spectroscopic studies in the 3300–3600 cm^{-1} region show that the band half-width of the overall band and the ratio of the integrated intensity of the modes of hydrogen bonding for OH stretch were discontinuous at the crystalline–CrG (or CrH), CrG (or CrH)–SmA and SmA–N transitions. Free OH groups formed upon entering the SmA phase. These results indicate that the hydrogen bonding of the terminal OH groups in these compounds may be the important factor dominating the morphology of the liquid crystal phases. The plot of the band half-width of the overall band for OH stretching changes with temperature and is proposed as a probe for the onset of phase transitions, each phase being thermodynamically stable within certain temperature ranges.

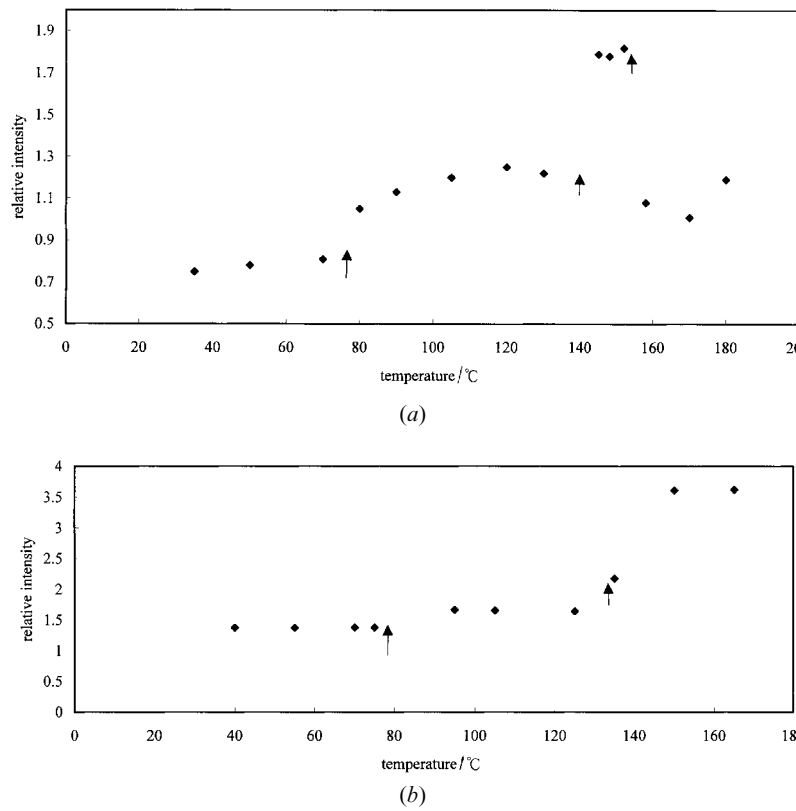

Figure 13. (*a*) Plot of relative intensity of the 1254 cm^{-1} band (reference band at 1278 cm^{-1}) vs. temperature for HAMS-4. (*b*) Plot of relative intensity of the 1258 cm^{-1} band (reference band at 1278 cm^{-1}) vs. temperature for HAMS-8.

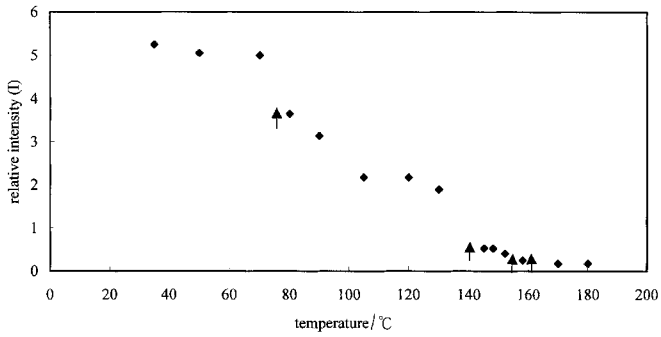

(*a*)

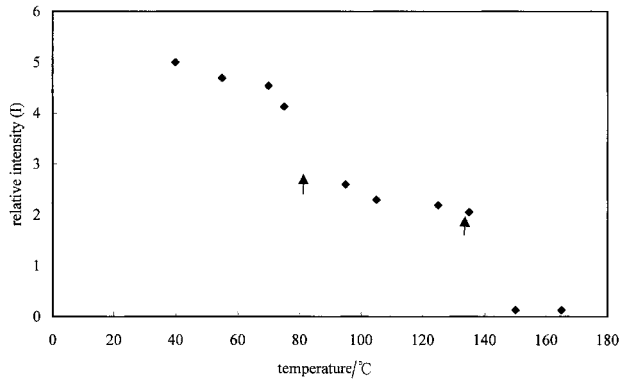

(*b*)

Figure 14. (*a*) Relative intensity of the 619 cm^{-1} band (reference band is the 639 cm^{-1} band) for HAMS-4 as a function of temperature. (*b*) Relative intensity of the 621 cm^{-1} band (reference band is the 639 cm^{-1} band) for HAMS-8 as a function of temperature.

As in earlier literature reports [4–6, 15], the spectra for the bending and rocking progression of the CH_2 moieties as a function of temperature suggest the onset of changes in the conformation of the alkyl terminal chain at the temperatures associated with the phase transitions. The spectra for the aromatic ring C=C stretch and the ring skeletal vibrations as functions of temperature provide some information about the onset of motion of the aromatic mesogenic core.

This research was undertaken with the financial support of Grant NSC-87-2216-E-006-007.

References

[1] Zerbi, G., Magni, R., Gussoni, M., Moritz, K. H., Bigotto, A. B., and Dirlikov, S., 1981, *J. chem. Phys.*, **75,** 3175.
[2] Zerbi, G., 1983, in *Advances in Infrared and Raman Spectroscopy*, Vol. 11, edited by R. J. H. Clark and R. E. Hester (London: Heyden), p. 301.
[3] Zerbi, G., 1983, in *Advances in Chemistry Series*, Vol. 203 (Washington, DC: American Chemical Society), p. 487.
[4] Galbiati, E., and Zerbi, G., 1986, *J. chem. Phys.*, **84,** 3509.
[5] Galbiati, E., and Zerbi, G., 1986, *J. chem. Phys.*, **87,** 3653.
[6] Kardan, M., Reinhold, B. B., Hsu, S. L., Thakur, B., and Lillya, C. P., 1986, *Macromolecules*, **19,** 616.
[7] Gray, G. W., and Jones, B., 1955, *J. chem., Soc.*, 4539.
[8] Jeffrey, G. A., 1986, *Acc. chem. Res.*, **19,** 168.
[9] Kato, T., and Frechet, J. M. J., 1990, *Maromolecules*, **23,** 360.
[10] Kato, T., and Frechet, J. M. J., 1989, *J. Am. chem. Soc.*, **111,** 8533.
[11] Kato, T., Adachi, H., Fujishima, A., and Frechet, J. M. J., 1992, *Chem. Lett.*, 256.
[12] Tschierske, C., Brezesinski, G., Kuschel, F., and Zaschke, H., 1989, *Mol. Cryst. liq. Cryst.*, **6,** 139.
[13] Qui, H., Li, M., Chen, X., Jing, F., and Zhou, E., 1998, *Liq. Cryst.*, **25,** 419.
[14] Li, M., Qui, H., Chen, X., Li, G., and Zhou, E., 1999, *Liq. Cryst.*, **26,** 1053.
[15] Smyth, G., Pollack, S. K., MacKnight, W. J., and Hsu, S. L., 1990, *Liq. Cryst.*, **7,** 839.
[16] Wan, C. H., Kuo, J. F., and Chen, C. Y., 2000, *Liq. Cryst.*, **27,** 523.
[17] Zaheer, S. H., and Bhushan, B., 1953, *Nature*, **171,** 746.
[18] Zaheer, S. H., Singh, B., Bhushan, B., Bhargava, P. M., Kacker, I. K., Ramachandran, K., Sastri, V. D., and Rao, N. S., 1954, *J. chem. Soc.*, 3360.
[19] Rotz, U., Lindau, J., Weissflog, W., Reinhold, G., Unseld, W., and Kuschel, F., 1989, *Mol. Cryst. liq. Cryst.*, **170,** 185.
[20] Goodby, J. W., 1998, in *Handbook of Liquid Crystals*, Vol. 2A, edited by D. Demus, J. W. Goodby, G. W. Gray, H.-W. Spiess, and V. Vill (Weinheim: Wiley-VCH), p. 426.
[21] Pugh, C., and Kriste, A. L., 1998, in *Handbook of Liquid Crystals*, Vol. 3, edited by D. Demus, J. W. Goodby, G. W. Gray, H.-W. Spiess, and V. Vill (Weinheim: Wiley-VCH), p. 156.
[22] Reck, B., and Ringsdorf, H., 1985, *Makromol. Chem. rapid Commun.*, **6,** 291, 691.
[23] Stenhouse, P. J., Valles, E. M., MacKnight, W. J., and Kantor, S. W., 1989, *Macromolecules*, **22,** 1467.
[24] Cox, R. J., Young, W. R., and Aviram, A., 1972, *J. Am. chem. Soc.*, **94,** 3976.
[25] Silverstein, R. G., Bassler, G. C., and Morrill, T. C., 1991, in *Spectroscopic Identification of Organic Compounds*, 5th Edn (John Wiley), pp. 109–112.
[26] Scherzer, T., 1994, *J. appl. Polym. Sci.*, **51,** 491.
[27] England-Kretzer, L., Fritzsche, M., and Luck, W. A. P., 1988, *J. mol. Struct.*, **175,** 277.
[28] Pimentel, G. C., and Sederholm, C. H., 1956, *J. chem. Phys.*, **24,** 639.
[29] Schactchneider, J. H., and Snyder, R. G., 1963, *Spectrochim. Acta*, **19,** 117.
[30] Snyder, R. G., 1967, *J. chem. Phys.*, **47,** 1316.
[31] Snyder, R. G., Hsu, S. L., and Krimm, S., 1978, *Spectrochim. Acta. A*, **34A,** 395.
[32] Seiber, R. H., 1969, *Liebigs Ann. Chem.*, **730,** 31.